Prion 4:4, 302-315; October/November/December 2010; © 2010 Landes Bioscience

Striatal pathology underlies prion infection-mediated hyperactivity in mice

Keith M. Gunapala,[1] Daniel Chang,[1] Cynthia T. Hsu,[1] Kebreten Manaye,[2] Ryan M. Drenan,[1] Robert C. Switzer[3] and Andrew D. Steele[1,*]

[1]Division of Biology; California Institute of Technology; Pasadena, CA USA; [2]Department of Physiology and Biophysics; College of Medicine; Howard University; Washington, DC USA; [3]Neurosciences Associates; Knoxville, TN USA

Key words: PrP, neurodegeneration, protein misfolding, home-cage, transmissible spongiform encephalopathy

Although prion diseases are most commonly modeled using the laboratory mouse, the diversity of prion strains, behavioral testing and neuropathological assessments hamper our collective understanding of mouse models of prion disease. Here we compared several commonly used murine strains of prions in C57BL/6J female mice in a detailed home cage behavior detection system and a systematic study of pathological markers and neurotransmitter systems. We observed that mice inoculated with RML or 139A prions develop a severe hyperactivity phenotype in the home cage. A detailed assessment of pathology markers, such as microglial marker IBA1, astroglial marker GFAP and degeneration staining indicate early striatal pathology in mice inoculated with RML or 139A but not in those inoculated with 22L prions. An assessment of neuromodulatory systems including serotonin, dopamine, noradrenalin and acetylcholine showed surprisingly little decline in neuronal cell bodies or their innervations of regions controlling locomotor behavior, except for a small decrease in dopaminergic innervations of the dorsal striatum. These results implicate the dorsal striatum in mediating the major behavioral phenotype of 139A and RML prions. Further, they suggest that measurements of activity may be a sensitive manner in which to diagnose murine prion disease. With respect to neuropathology, our results indicate that pathological stains as opposed to neurotransmitter markers are much more informative and sensitive as markers of prion disease in mouse models.

Introduction

Prions are infectious particles composed of misfolded protein that cause a collection of disorders known as prion diseases or transmissible spongiform encephalopathies.[1-4] Prion diseases are acquired genetically, spontaneously or through exposure to infectious material. The hallmark features of prion disease are the misfolding of the cell surface prion protein (PrP), dementia, ataxia and subsequently death.

In contrast to many neurodegenerative diseases, the cardinal aspects of prion disease can be recapitulated accurately in the mouse in terms of the pathological and biochemical changes in the brain. Recent efforts demonstrate the ability to spontaneously generate prions from recombinant protein[5] or in mice expressing mutant PrP.[6,7] Another key advantage of studying prion disease in the mouse is the ease, succinctness and reliability with which models can be created simply by inoculating prions directly into the brains of inbred mouse strains. In such assays, wild-type or knockout mice are inoculated with established prion "strains." Strains of prions are defined by the amount of time it takes for mice to succumb to disease (termed "incubation time"), the pathological lesions and the migration of proteinase-K resistant PrP that they exert in hosts.[8,9] Efforts using mouse genetics to identify molecular pathways involved in prion toxicity[10-14] or therapy[15] highlight the importance of standardization of behavioral and pathological assessments in this system.

In this study, we utilized several prion strains to better understand the behavioral and neuropathological changes that occur in mouse models of prion disease. To that end, we performed a comparison of the three prion strains RML, 139A and 22L using normal brain homogenate injection as a control. We observed that RML and 139A prions cause a dramatic increase in activity as an early feature of prion disease whereas 22L prions cause an early onset hypoactivity. We sought to further characterize the locomotor circuitry and observed that pathological markers, such as stains for glial cells and silver staining for degenerating neurons, showed robust and early changes in locomotor regions but surprisingly, there was scant evidence for loss of cell types mediating locomotor behavior, including parvalbumin, dopamine, noradrenaline, serotonin and acetylcholine marker positive neurons and/or innervations.

Results

Lifespan and homeostatic behaviors. Mice were inoculated intracranially with a normal brain homogenate (NBH) (0.01%),

*Correspondence to: Andrew D. Steele; Email: steelea@caltech.edu
Submitted: 09/02/10; Accepted: 09/22/10
Previously published online: www.landesbioscience.com/journals/prion/article/13721
DOI: 10.4161/pri.4.4.13721

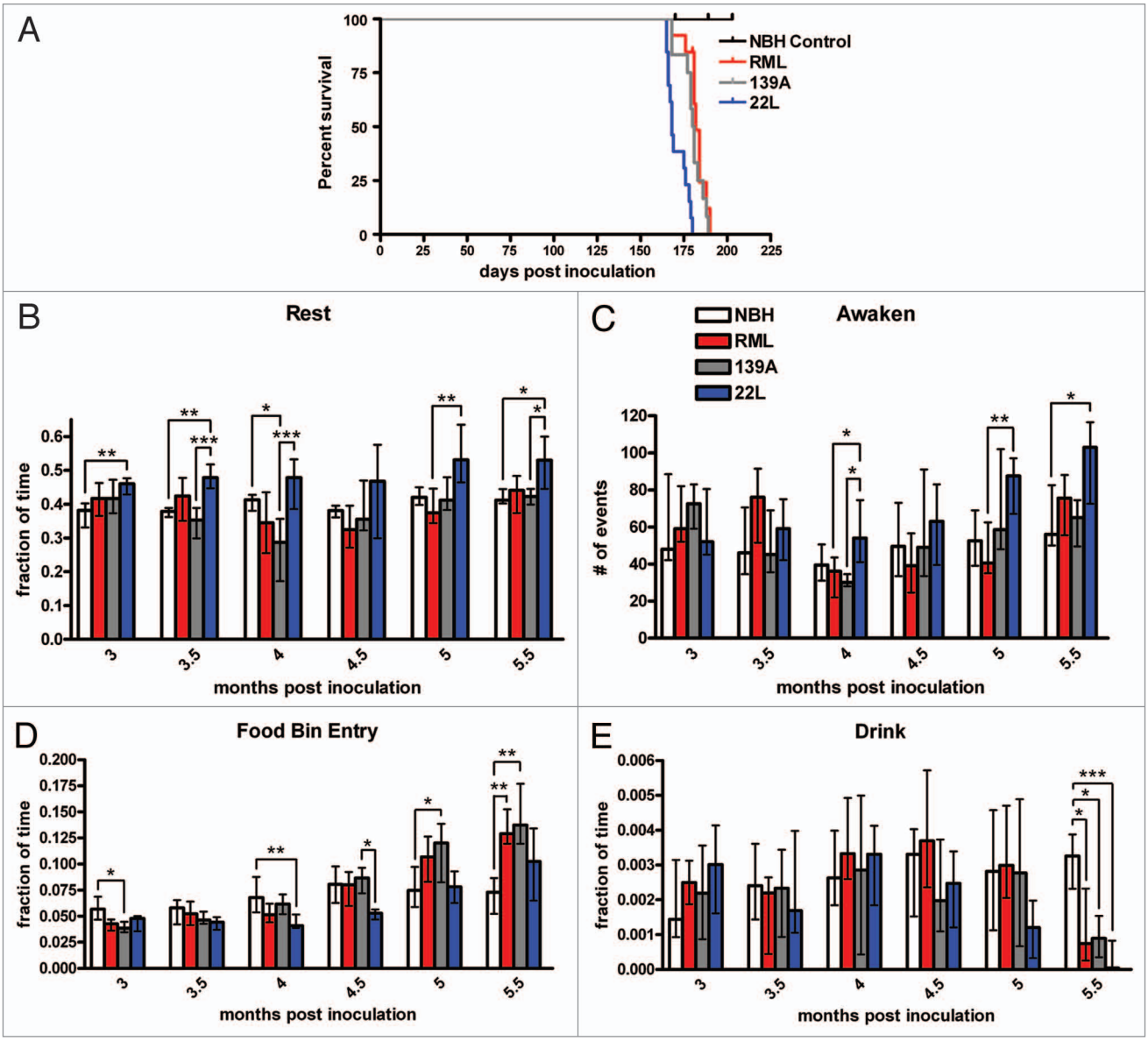

Figure 1. Lifespan and homeostatic behaviors of prion-inoculated mice. (A) RML-, 139A- and 22L-inoculated mice have a narrow mortality window between 175–200 days post inoculation. NBH vehicle control mice are euthanized at times indicated with a tick mark. (B) The fraction of total time spent in a resting state (nearly complete immobility for >30 seconds). (C) The number of events of awakening, which is the termination of a resting state. (D) Fraction of total time spent entering the food bin. (E) The fraction of total time spent drinking. All statistical comparisons were done using the Kruskal-Wallis test with post-test (*$p < 0.05$; **$p < 0.01$; ***$p < 0.001$).

139A prions, RML prions or 22L prions. 22L-inoculated mice were the first to show a decrease in survival while RML and 139A-inoculated mice followed very soon afterwards but were slightly delayed in their mortality rate (**Fig. 1A**). All three groups had a very narrow window of approximately 2 weeks in which the percent survival plummeted from 100–0%. NBH control mice could live well beyond the survival threshold of prion inoculated mice; however, these mice were sacrificed during and after the time at which prion-inoculated mice succumbed to disease.

We characterized the home cage behavior of the mice using a computer vision system (HomeCageScan 2.0), to observe behavioral changes associated with prion pathology. The first behavioral measurement was made 1 month after inoculation, during which there were no significant differences in behavior between the four groups (not shown) and subsequently the mice were video recorded at 3 months post inoculation (mpi) until 5.5 mpi at 2 week intervals. We initially examined several homeostatic behaviors including resting, awakening, food bin entry and drinking. 22L-inoculated mice had significantly more resting compared to the NBH vehicle control at several time points, 3, 3.5 and 5.5 mpi (**Fig. 1B**). RML- and 139A-inoculated mice showed relatively similar fraction of time resting compared to

the NBH control with the exception of 4 mpi where 139A had a statistically significant decrease in the fraction of time resting (**Fig. 1B**).

To examine the number of resting states we quantified the amount of "awakening" events, which represent a disruption in a resting state. We observed very few alterations in the number of awakening events between all prion-inoculated mice and controls, despite a trend towards increased awakening in 22L-inoculated mice. The only significant change in awakening occurred at 5.5 mpi where 22L had a statistically significant increase in awakening relative to the control mice (**Fig. 1C**). Given that 22L mice spent more total time resting it is not surprising that they showed increase awakening events as the definition of awaken is the termination of a resting state.

At 3 mpi there was a statistically significant decrease in food bin entry in 139A inoculated mice; however, at each 2 week measurement food bin entry increased in 139A-inoculated mice until 5 and 5.5 mpi when the increase in food bin entry relative to NBH controls became statistically significant (**Fig. 1D**). RML food bin entry only became significantly higher than the NBH control at 5.5. 22L-inoculated mice never showed an increase over control food bin entry levels and did show a significant decrease at one time point, 4 mpi (**Fig. 1D**).

Finally, the fraction of time spent drinking differed only at the near terminal stage of disease, 5.5 mpi, when all three pathogenic prion groups had a statistically significant reduction in drinking relative to the NBH control (**Fig. 1E**).

Major activity behaviors in the home cage. NBH control mice had little variation in the amount of distance traveled (around 1,000 meters) in the 24 h observation period from 3–5.5 mpi. 22L-inoculated mice showed an early hypoactivity phenotype, traveling significantly less distance relative to the NBH control at 3 and 3.5 mpi (**Fig. 2A**). From 4 mpi onward, 22L had no statistically significant difference compared to the NBH control. RML and 139A were not significantly different relative to the NBH control at 3 and 3.5 mpi. Strikingly, at 4 mpi and onward, both RML and 139A showed a sharp increase in distance traveled (**Fig. 2A**). Another metric of activity, jumping, was not significantly different between the three prion strains and the NBH control at 3 mpi but noticeable changes begin at 3.5 mpi onwards. At 3.5 mpi, 22L had a significant decrease in jumping relative to the control, confirming the slight hypoactivity phenotype observed with distance traveled. At 4 mpi, there was a noticeable increase in jumping for both RML and 139A yet 139A is the only strain with a significant increase in jumping relative to the control (**Fig. 2B**). Interestingly, another metric of activity, hanging behaviors, were markedly decreased in all prion-inoculated mice beginning at 4.5 mpi (**Fig. 2C**). The trends for hang vertically were almost identical to those of hang cuddled (**Fig. 2D**).

At early time points (from 3–3.5 mpi) grooming was very similar between the three prion groups and the NBH control. At 4 mpi and beyond, RML and 139A exhibited significantly less grooming than the control although 22L remained level with NBH. At 4.5 months, the time spent grooming was significantly less than NBH in all three strains and this trend continued to 5 and 5.5 mpi. Unlike hang cuddled and hang vertical, which cease entirely in prion-infected mice at 4.5 mpi, grooming steadily declined from 4 mpi onward (**Fig. 2E**). In fact, for RML and 139A decreased grooming is at least as sensitive a diagnostic as increased distance traveled. At 3 and 3.5 mpi, 22L had lower rearing than the NBH control, suggesting further that 22L prions caused a hypoactivity phenotype early in disease (**Fig. 2F**).

Temporal distribution of activities. To simultaneously examine a number of different home cage activity parameters and their distributions with respect to light and dark cycle, we created "stacked" behavior plots. In these diagrams, the median value for each behavior is stacked one on top of the other, such that their summation is the peak of activity overall but each component can be visualized by its respective color (**Fig. 3A**). At 3 mpi, the NBH control, RML, 139A and 22L had a relatively similar distribution of time spent engaging in most behaviors and show a general night-time peak of activity and decline in activity during the light cycle. At 5 mpi, the distribution of behaviors in the NBH control mice was similar to that of the control at 3 mpi; however, RML and 139A showed both an overall increase in the night-time peak with increases specifically in walking and food bin entry. 22L at 5 mpi had noticeable increases in walking and food bin entry but there appears to be a shift in the distribution of most of the high activity occurring in the late phase of the dark cycle (as opposed to at 3 mpi where the bulk of the activity in the dark cycle occurred at the beginning when lights were turned off) (**Fig. 3A**).

To probe further the hyperactivity phenotype observed in RML and 139A-inoculated mice, we created another visualization of the distance traveled data where the median value in distance traveled per hour is represented in an intensity map for all time points measured. Thus, one can examine this metric at all time points across the circadian cycle (**Fig. 3B**). From hours 0–2 (0 being the start of the recording period) there was a slight increase in median distance traveled for all four groups at all times except for late in disease. Control animals typically had the highest median levels of distance traveled (between 50–100 meters per hour) during hours 4–8. 22L-inoculated mice traveled a median of 50–100 meters per hour between hours 2–14 inclusive (a wider time frame than controls) into the recording from time points 4–5 mpi. RML and 139A-inoculated mice increased distance traveled from hours 6–14, traveling between 150 and 350 meters an hour, during 4–5.5 mpi. Overall, this representation shows that RML and 139A had a shift to a late night activity peak as well as an increased magnitude relative to both NBH and 22L (**Fig. 3B**).

Degeneration and gliosis in the dorsal striatum. Separate cohorts of animals were culled at 4, 4.5, 5 and 5.5 mpi for neuropathological analysis (n = 2 per group per time point). Ag-Cu staining (**Fig. 4A and B**) was used to identify degenerating neuronal cell bodies and terminals.[16-18] Interestingly, we noted that RML- and 139A-inoculated mice had an increase in staining intensity relative to NBH control in the dorsal striatum, a region known to be involved in locomotor behavior (**Fig. 4D**).[19,20] To quantify the degeneration in the dorsal striatum, low magnification images where obtained (**Fig. 4B**) and staining intensity

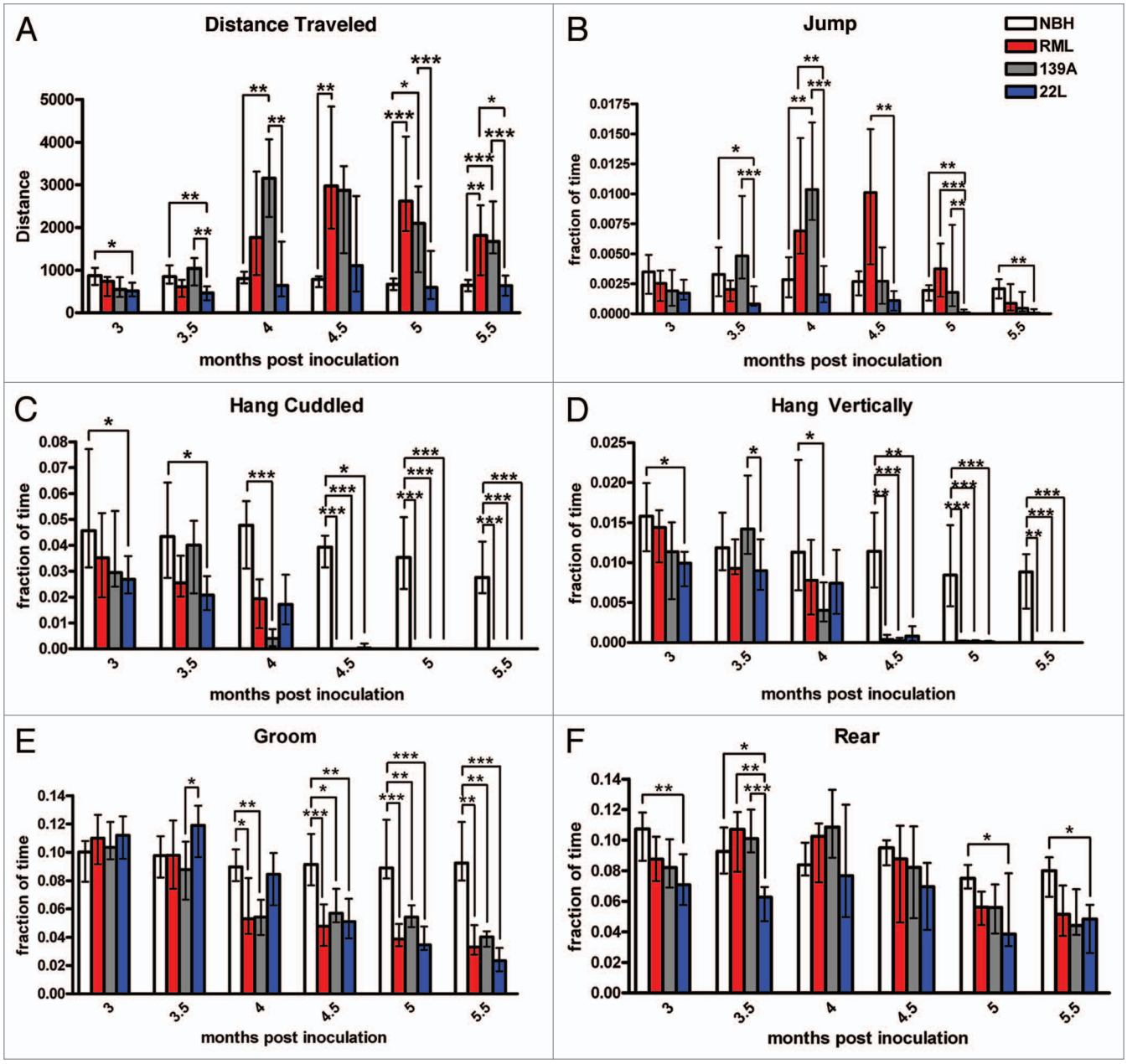

Figure 2. Major activity behaviors of prion-inoculated mice. (A) Total distance traveled in the 24 hour video recording. (B) The fraction of total time spent jumping. (C) The fraction of total time spent hang cuddling, or upside down. (D) The fraction of total time spent hanging vertically. (E) The fraction of total time spent grooming. (F) The fraction of time spent rearing. All statistical comparisons were done using the Kruskal-Wallis test with post-test (*$p < 0.05$; **$p < 0.01$; ***$p < 0.001$).

measurements (**Fig. 4C**) were acquired using Nikon Elements software to determine percent area of the dorsal striatum that was stained for such degeneration. 139A-inoculated mice at 4 mpi showed a statistically significant level of degeneration staining relative to the NBH control. At 4.5 mpi, there was clear degeneration of dorsal striatum in all pathological prion stains (RML, 139A and 22L). At 5 mpi RML- and 139A inoculated mice still had statistically significant degeneration, but 22L-inoculated mice no longer had statistically significant degeneration relative to the NBH control. At 5.5 mpi, all three prion strains had highly statistically significant degeneration in the dorsal striatum relative to the NBH control (**Fig. 4D**).

As a next step in corroborating the dorsal striatum as a pathogical "hotspot," we quantified staining of glial cells in the dorsal striatum. We noticed increased levels of gliosis for both astroglia and microglia in the dorsal striatum (**Fig. 4E–H** for IBA1 staining, L and M for GFAP staining). We quantified the IBA1 microgliosis by counting individual cells in the dorsal-medial portion of the dorsal striatum (**Fig. 4I**) and discovered that RML- and 139A-inoculated mice had statistically increased IBA1 gliosis

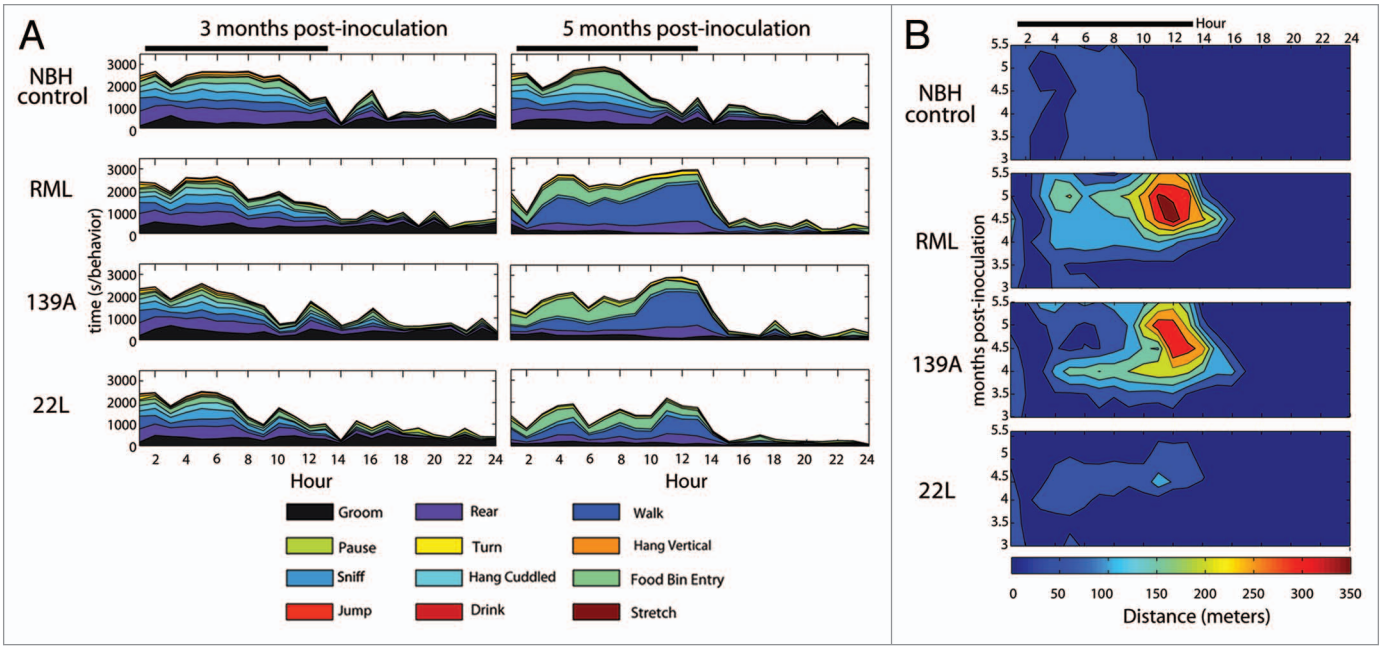

Figure 3. (A) Stacked activity plot showing the median number of seconds per hour the mice in each experimental group exhibit selected activities at 3 mpi (left part) and 5 mpi (right part). The behaviors shown include groom, rear, walk, sniff, hang cuddled, hang vertical, food bin entry, pause, turn, jump, drink and stretch each denoted by a different color (see key). Behaviors identified by HomeCageScan but not included as an activity were awaken, chew, rest, twitch and remain low. The black bar indicates the dark cycle. (B) Intensity plot showing how the median distance traveled within a 24 h period varies over the duration of the experiment (from 3–5.5 mpi; each time point represents, n = 11–13 mice). Blue and green coloration indicates distances of 150 meters traveled or less and yellows, oranges and red indicate distance of 200 meters or higher traveled. The black bar indicates the dark cycle.

beginning at 4 mpi whereas 22L had a delayed onset beginning at 5 mpi. To verify the accuracy of our manual cell counts, we also quantified the percentage of area stained using densitometry with software as was used in quantifying Ag-Cu degeneration staining above. The percent area of IBA1 staining in the dorsal striatum gave nearly identical results as did manual counting, with significantly increased gliosis of RML and 139A relative to control at 4 mpi. In contrast, 22L inoculation did not lead to substantial microgliosis in the dorsal striatum although there is a small trend toward an increase (**Fig. 4J**). As a further confirmation on our methodology, unbiased stereology on several samples showed similar trends to both densitometry and manual cell counts (**Fig. 4K**).

To assess further the neurodegeneration in the dorsal striatum, we next quantified GFAP-positive astroglia (**Fig. 4L and M**). We performed both manual cell counts and densitometry measurements of GFAP-positive astroglia. In control samples, there was very little GFAP staining in the dorsal striatum for all time points examined (**Fig. 4N and O**). At time points of 4, 4.5 and 5 mpi there was a marked increase in the cell count (**Fig. 4N**) and percent area (**Fig. 4O**) of the dorsal striatum stained for GFAP in the RML- and 139A-inoculated mice relative to the NBH control. In contrast, 22L-inoculated samples had very little astrogliosis at the earlier time points. By 5 mpi, there were high levels of GFAP staining in all prion-inoculated mice (**Fig. 4N and O**), which is reflective of a global increase in gliosis (both astro- and microglia) that occurs in all brain regions (data not shown).

Dopaminergic innervation of the dorsal striatum. We next sought to determine which neurotransmitter systems affecting locomotor regions were affected in the RML- and 139A-inoculated animals, which show a dramatic hyperactivity phenotype. Given the major innervations of the dopaminergic system to the striatum from the substantia nigra (SN) in the midbrain,[19] we stained for a marker of dopamine neurons, tyrosine hydroxylase (TH) (**Fig. 5A and B**). At time points 4, 4.5 and 5 mpi, there were no statistically significant differences between TH positive neuron counts in the SN pars compacta of the NBH controls versus the RML, 139A and 22L inoculated mice (**Fig. 5C**).

Intensity measurements of percent area of the dorsal striatum stained for TH were obtained (**Fig. 5D–F**). Interestingly, dopaminergic innervations of the dorsal striatum in 139A inoculated mice were decreased from 4 mpi onward. The dopaminergic innervations to the dorsal striatum of the RML inoculated mice decreased significantly at 4.5 and 5 mpi while 22L inoculated mice had no changes in dopaminergic innervations to the dorsal striatum (**Fig. 5G**).

Serotonergic innervation of the dorsal striatum and midbrain. Given that (1) lesions to the serotonergic system cause hyperlocomotion in mice,[21] (2) serotonin has broad modulating effects on many nuclei and (3) serotonin is co-released with dopamine from dopaminergic terminals in the striatum[22] and (4) early dysfunction in the serotonin system was documented in mouse model of bovine spongiform encephalopathy,[23] we next investigated the serotonergic system. Most serotonergic neurons

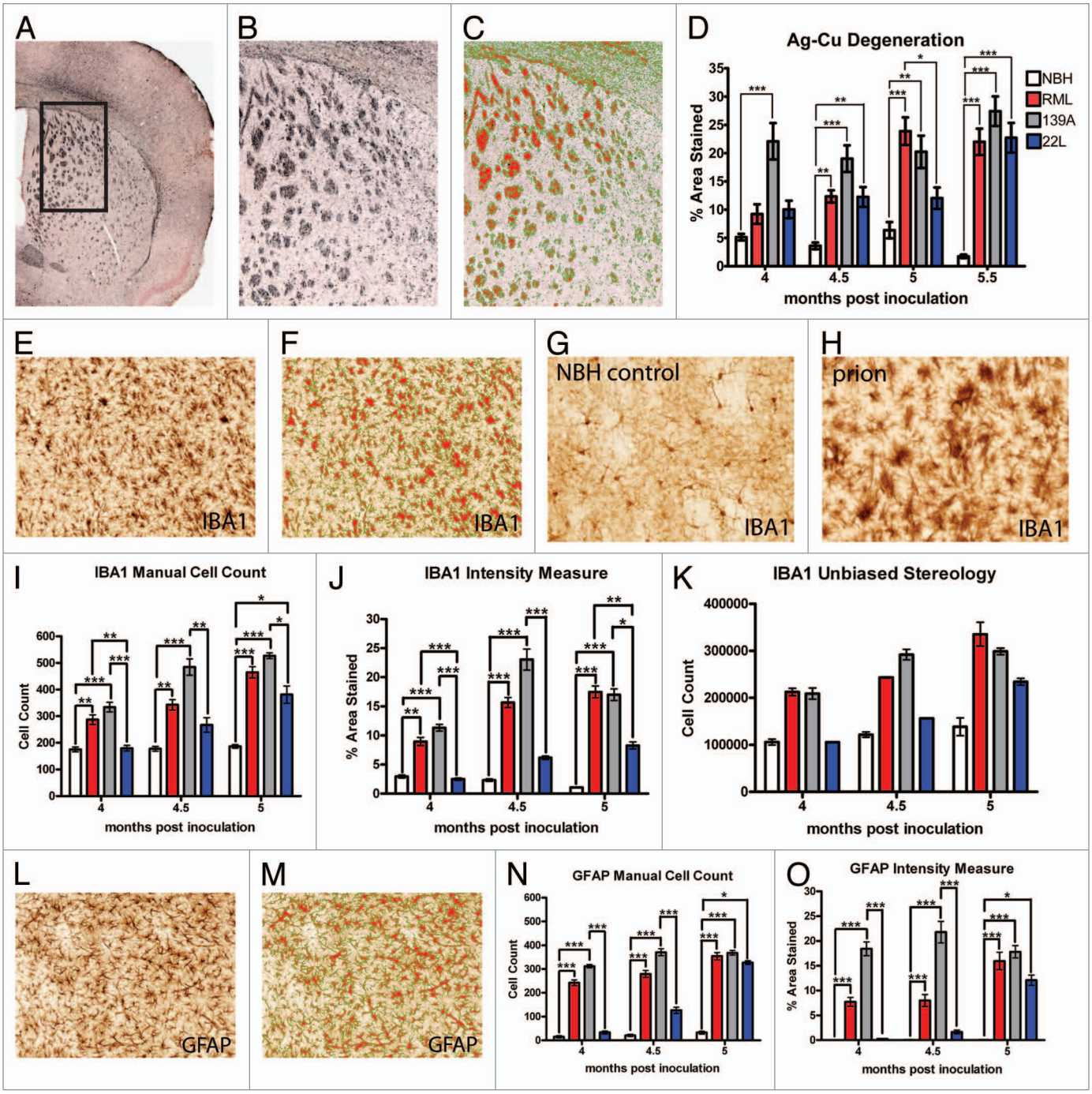

Figure 4. Degeneration and gliosis in the dorsal striatum. (A) Ag-Cu degeneration stained representative image (low magnification) of the dorsal striatum and at (B) higher magnification and (C) an image of the Nikon Elements software automated quantitation. (D) Mean percentage area stained. (E) Representative images of IBA1 stained dorsal striatum (F) and the software intensity measurement. Representative higher magnification images of IBA positive microglia in (G) NBH controls, note the paucity of cell bodies and the smaller size of processes than what is seen in representative (H) prion-inoculated mice which have more IBA1 signal and larger cell size. (I) Mean manual cell counts and (J) % area stained measures of IBA1 positive microglia in the dorsal striatum. (K) Unbiased stereology of IBA1 positive microglia in the dorsal striatum. Representative images of GFAP-stained dorsal striatum at (L) and the (M) automated software measurement of staining. (N) Mean manual cell counts and (O) intensity measures of GFAP positive astrocytes in the dorsal striatum. All statistical comparisons were done using the Kruskal-Wallis test with post-test (*$p < 0.05$; **$p < 0.01$; ***$p < 0.001$).

are localized in the dorsal raphe nucleus (DRN) and identified by staining for serotonin (5HT) (**Fig. 6A and B**). Surprisingly, there were no statistically significant changes in 5HT positive neuron counts in the DRN of any prion-inoculated strain relative to the control at any time points (**Fig. 6C**). Since the soma of the serotonin neurons were intact, we examined serotonergic innervations

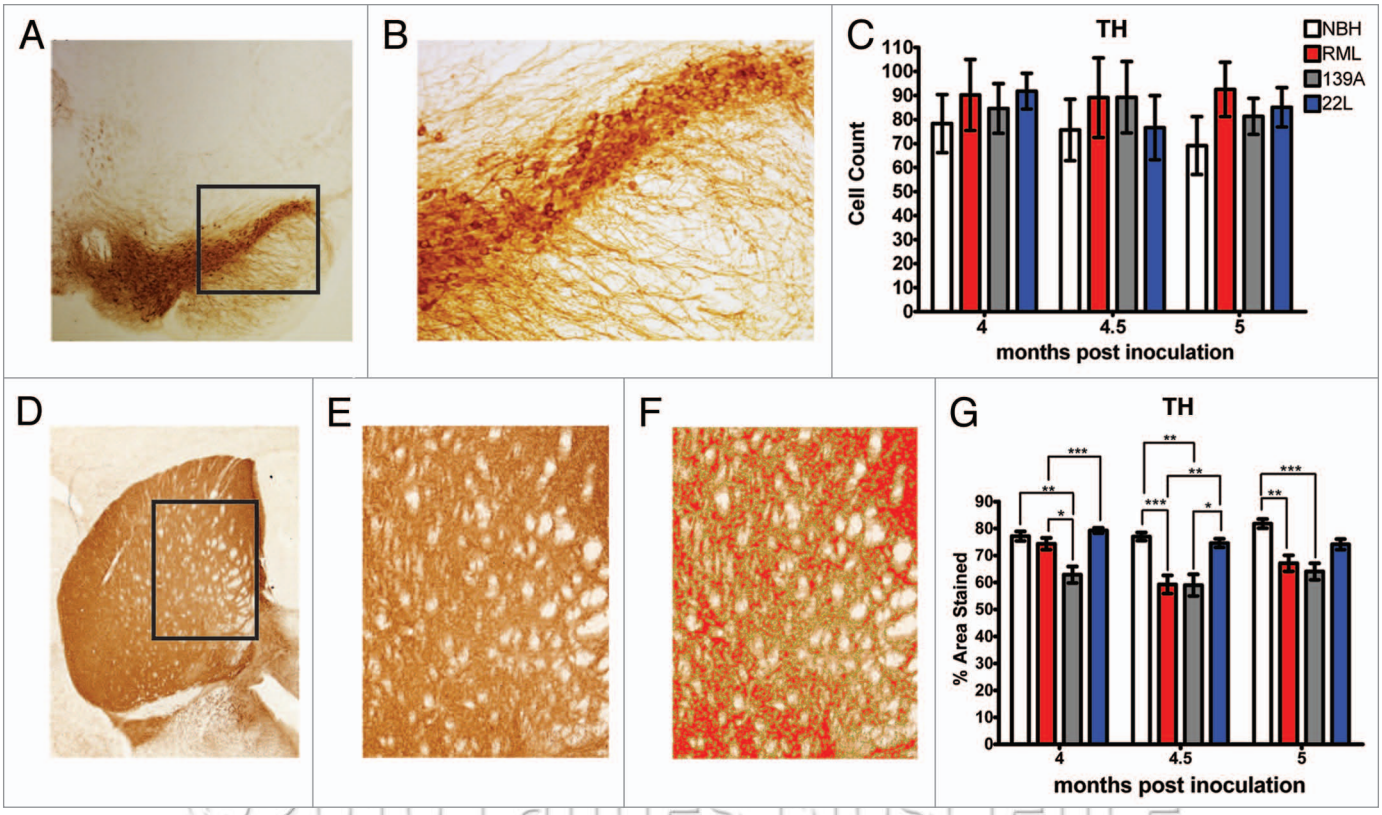

Figure 5. Dopaminergic neurotransmitter system innervations of the dorsal striatum and cell counts. (A) Representative low magnification image of the substantia nigra, stained for tyrosine hydroxylase (TH) and (B) at higher magnification used to count cells. (C) TH positive cell counts in the substantia nigra were not significantly changed. (D) Representative images of the dorsal striatum, stained for TH and at higher magnification (E) used to quantify innervation, a representative intensity measurement is shown in (F). (G) Dopaminergic innervations in the dorsal striatum are significantly decreased in RML and 139A inoculated mice. All statistical comparisons were done using the Kruskal-Wallis test with post-test (*$p < 0.05$; **$p < 0.01$; ***$p < 0.001$).

of the dorsal striatum (**Fig. 6D–F**). Beginning at 4.5 mpi, RML showed the first signs of having a statistically significant decrease in serotonergic innervations in the dorsal striatum that continues to 5 mpi (**Fig. 6G**). Overall, it appeared that prion inoculation of the RML strain subtly modifies serotonergic innervations of the dorsal striatum while the other strains had no statistically significant changes in the serotonergic innervations of the dorsal striatum (**Fig. 6G**). Finally, because serotonergic neurons innervate the SN (including the pars compacta and reticulata) (**Fig. 6H–J**) we quantified serotonergic innervations of the SNc/r (**Fig. 6K**). Overall, there was no statistically significant difference between groups for innervations of the SNc/r in the NBH control versus the serotonergic innervations of the SNc/r in the other three pathological strains. Thus, as for serotonergic innervations of the dorsal striatum, the innervations of the SNc/r were preserved and intact (**Fig. 6K**).

Parvalbumin GABAergic inhibitory neurons in the dorsal striatum and substantia nigra. Given that the dopaminergic and serotonergic systems appeared fairly intact, we reasoned that a loss of inhibitory inputs on the locomotor system could also explain the hyperactivity phenotype observed in RML- and 139A-inoculated mice. Therefore, we assessed the state of a subset of GABAergic inhibitory neurons in the dorsal striatum, using parvalbumin as a marker (**Fig. 7A and B**). Previous reports have indicated a loss of parvalbumin-positive neuron in the cortex and hippocampus of humans suffering from prion disease.[24] Oddly, at 4 mpi there was a small but significant increase in parvalbumin-positive neurons for 139A and this was true for RML samples at 4.5 and 5 mpi (**Fig. 7C**) while there was significant loss of these cells compared to controls at any time point.

One possible explanation for the hyperactivity associated with RML and 139A was less inhibition of dopamine neurons within the SN that could be caused by the loss of the inhibitory neurons in the ventral midbrain. To that end, we examined parvalbumin-stained sections of the SNc/r (**Fig. 7D–E**). At 4 mpi there was a statistically significant decrease in parvalbumin-positive cells in RML-inoculated mice relative to the NBH control but this difference was not sustained at 4.5 and 5 mpi. 139A-inoculated mice become hyperactive but had no loss (and even a trend toward increased) of parvalbumin cells (**Fig. 7F**). These results suggest that loss of parvalbumin neurons is not a general feature of murine prion disease as opposed to human samples.[25] We also stained for Calbindin-positive neurons to test for a loss of this subset of GABAergic neurons but these cells were not present in either the dorsal striatum of ventral midbrain despite their presence elsewhere in the brain (data not shown).

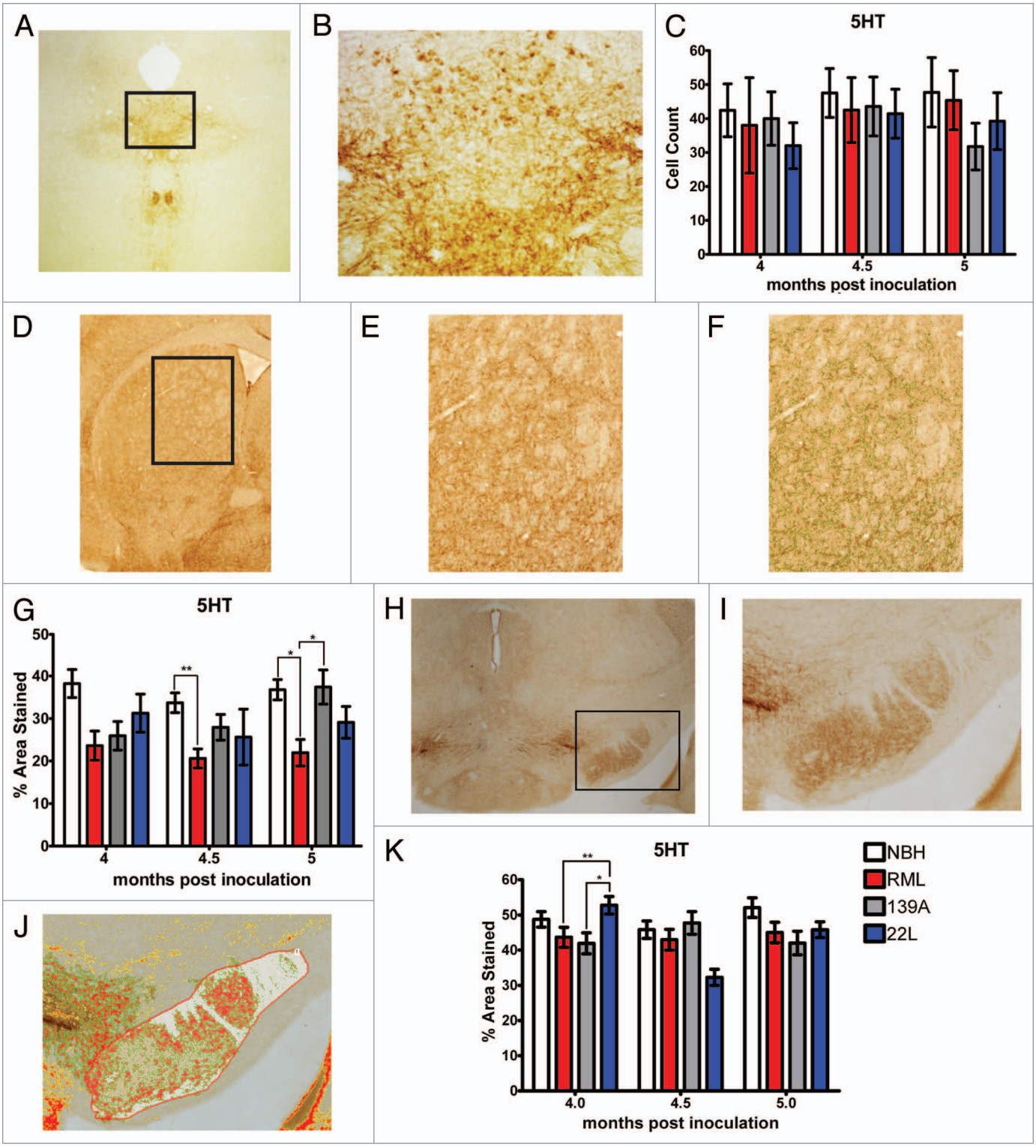

Figure 6. Serotonin system in prion-infected mice. (A) Representative images of the dorsal raphe nucleus (DRN), stained for serotonin (5HT). (B) Higher magnification of the DRN used to count cells. (C) 5HT-positive cell counts in the DRN. (D) Representative low magnification image of the dorsal striatum, stained for 5HT and (E) at higher magnification (10x) used to quantify 5HT neuronal processes as shown in (F). (G) Serotonergic innervations to the dorsal striatum. (H–J) Representative images of the substantia nigra, stained for serotonin. (K) Serotonergic innervations to the substantia nigra. All statistical comparisons were done using the Kruskal-Wallis test with post-test (*$p < 0.05$; **$p < 0.01$).

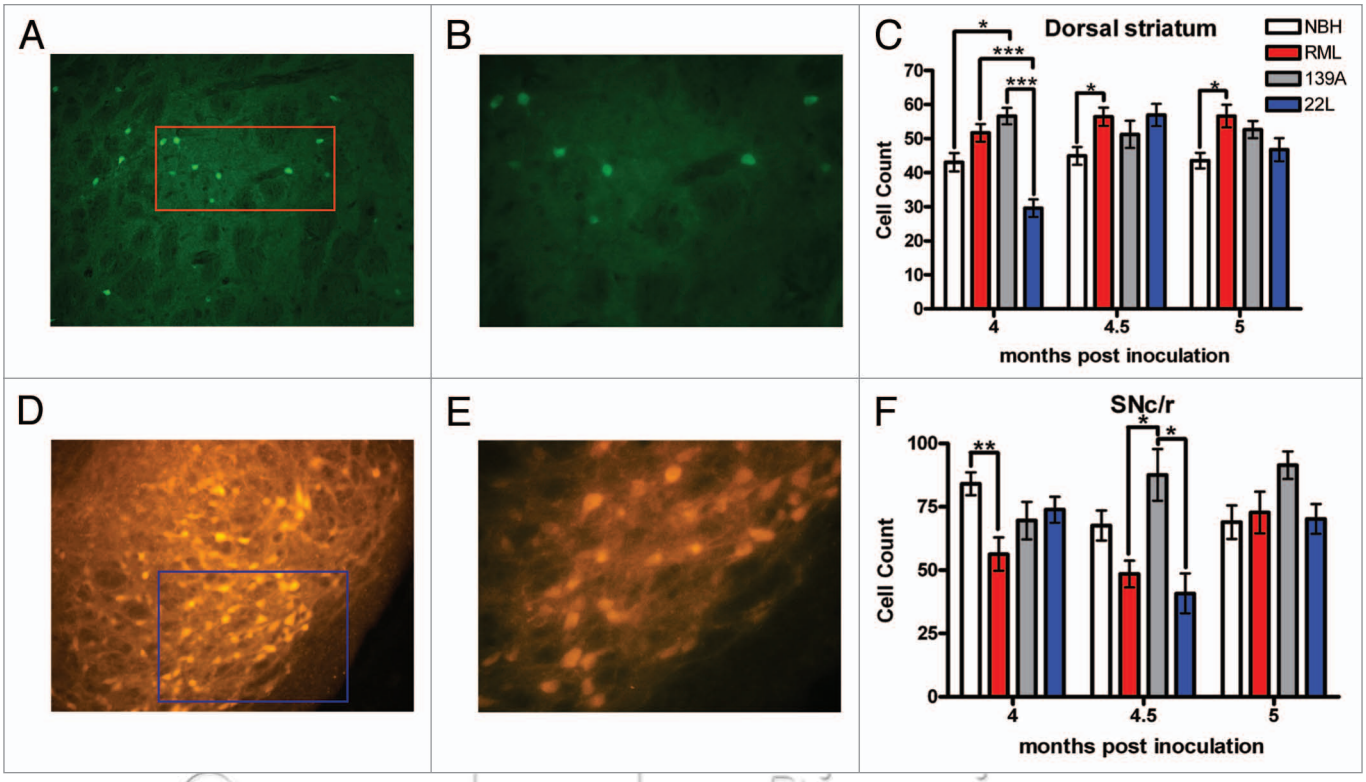

Figure 7. Quantification of parvalbumin-positive GABAergic neurons. (A) Representative image of parvalbumin staining in the dorsal striatum and (B) at magnification used to count cells. (C) Parvalbumin cell counts in the dorsal striatum. (D) Representative images of the parvalbumin staining in substantia nigra. (E) Representative image of parvalbumin staining used to count cells. (F) Parvalbumin cell counts in the substantia nigra. All statistical comparisons were done using the Kruskal-Wallis test with post-test (*p < 0.05; **p < 0.01; ***p < 0.001).

Cholinergic system in the dorsal striatum and brainstem. It has been well established that the cholinergic system is a major mediator of locomotor behavior and modifications to the cholinergic system often result in hyperactivity.[26-28] We used choline-acetyl transferase (ChAT) to mark the cholinergic system. We examined ChAT-positive neurons, "giant cholinergic" neurons, of the dorsal striatum (**Fig. 8A, B and D**). In terms of cell counts of giant cholinergic neurons, there was no change in the number of ChAT positive cells between the NBH controls and the experimental groups at any time point throughout the experiment, leading us to conclude that giant cholinergic neurons in the dorsal striatum were intact (**Fig. 8C**). Because cholinergic cell counts were intact in the dorsal striatum, we measured cholinergic innervations in the dorsal striatum. Low magnification images were used to identify a complete field to quantify cholinergic innervations (**Fig. 8E and F**). At 4 and 4.5 mpi, there was no significant difference between cholinergic innervations of the dorsal striatum in the NBH control relative to the prion groups, but at 5 mpi there was a statistically significant decrease in cholinergic innervation in the dorsal striatum of RML-inoculated mice whereas 139A- and 22L-inoculated mice had no changes in innervations relative to the control (**Fig. 8G**).

Two independent cholinergic nuclei were quantified for changes in cholinergic (ChAT positive) cell counts: the pedunculopontine tegmental nucleus (PPTg) (**Fig. 8H and I**) and the laterodorsal tegmental nucleus (LDTg) (**Fig. 8K and L**). There were no statistically significant changes in both ChAT-positive cell counts in either brain region (**Fig. 8J and M**). It appears that the ChAT-positive neurons of the PPTg and LDTg were both intact and not perturbed by the prion inoculation.

Noradrenergic neurons in the locus coeruleus. Noradrenergic neurons in the locus coeruleus are the only source of noradrenaline in the brain and project widely throughout the brain excepting the basal ganglia.[29] These neurons are very important in determining behavioral states, vigilance, stress response and even cognition.[29] Previous studies in mouse models of Alzheimer disease showed that these neurons are very prone to degeneration and loss in mouse models of Alzheimer disease[30] so we counted the number of noradrenergic neurons in the locus coeruleus, using TH as a marker (**Fig. 9A**). Both manual cell counts (**Fig. 9B**) and unbiased stereology (**Fig. 9C**) of TH-positive neurons demonstrated no significant changes in the number of noradrenergic neurons between the three prion strains and the NBH control.

Discussion

We observed that the commonly used prion stains RML and 139A caused a hyperactivity phenotype and this may be useful for monitoring therapeutic interventions or assessments of genetic pathways of neurotoxicity in mouse. The striking similarity between the behavior of 139A- and RML-inoculated mice is attributable to the fact that both are derived from the same

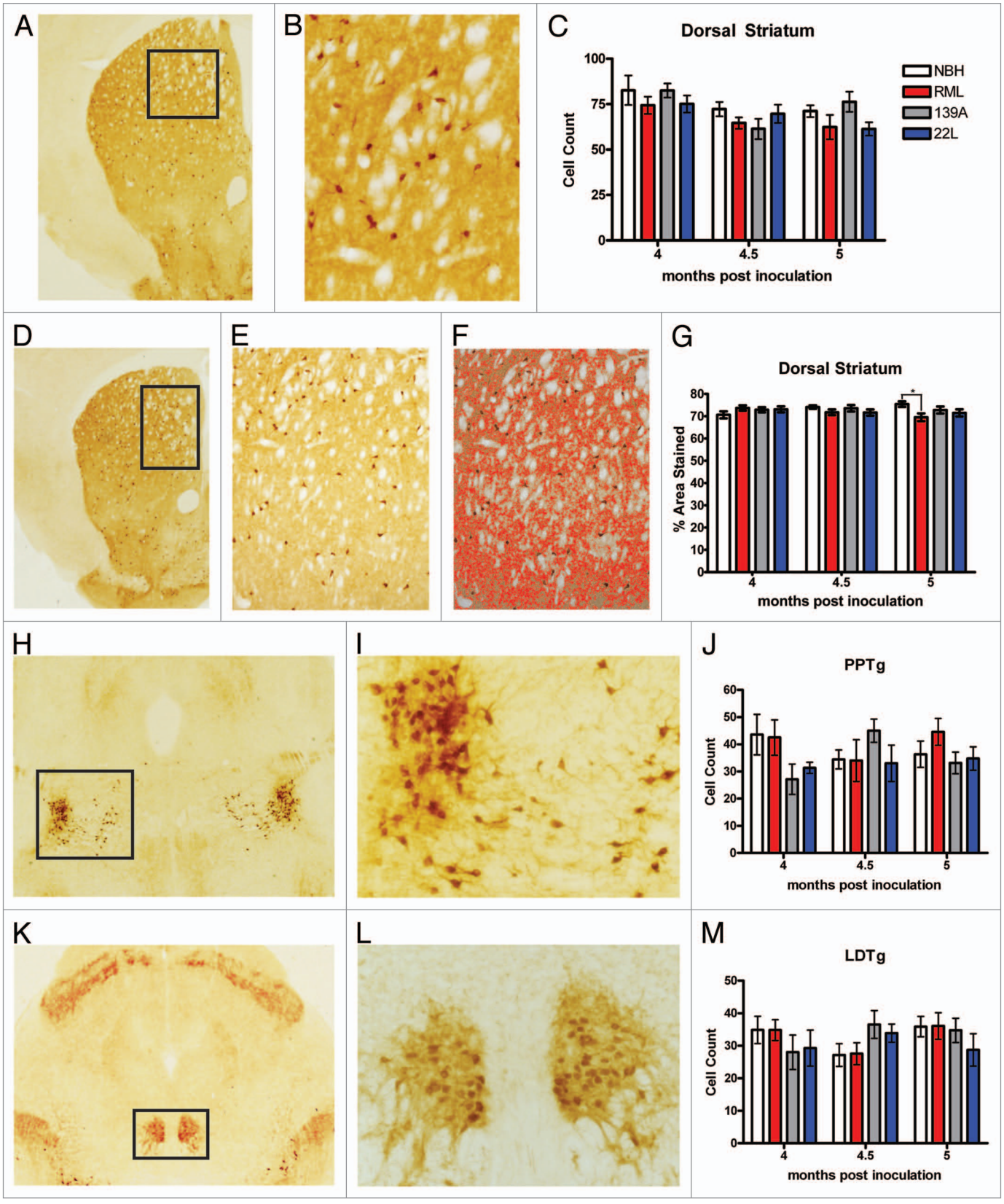

Figure 8. For figure legend, see page 312.

Figure 8 (See previous page). Quantification of the ChAT-positive cholinergic system. (A) Representative image of ChAT staining in striatum. (B) Higher magnification of ChAT staining used to count ChAT-positive giant cholinergic neurons. (C) ChAT-positive giant cholinergic neuron counts. (D) Representative image of the dorsal striatum used to quantify the ChAT-positive fibers. (E) Higher magnification used to quantify fibers using the automated software measurement shown in (F) which excludes the giant cholinergic cell bodies. (G) Cholinergic innervations in the dorsal striatum by the giant cholinergic neurons. (H) Representative images of the PPTg and (I) at higher magnification used to count cells. (J) ChAT-positive neuron count in the PPTg is not altered. (K) Representative images of the LDTg and (L) at higher power used to count cells. (M) ChAT-positive neuron count in the LDTg is not altered. All statistical comparisons were done using the Kruskal-Wallis test with post-test (*$p < 0.05$).

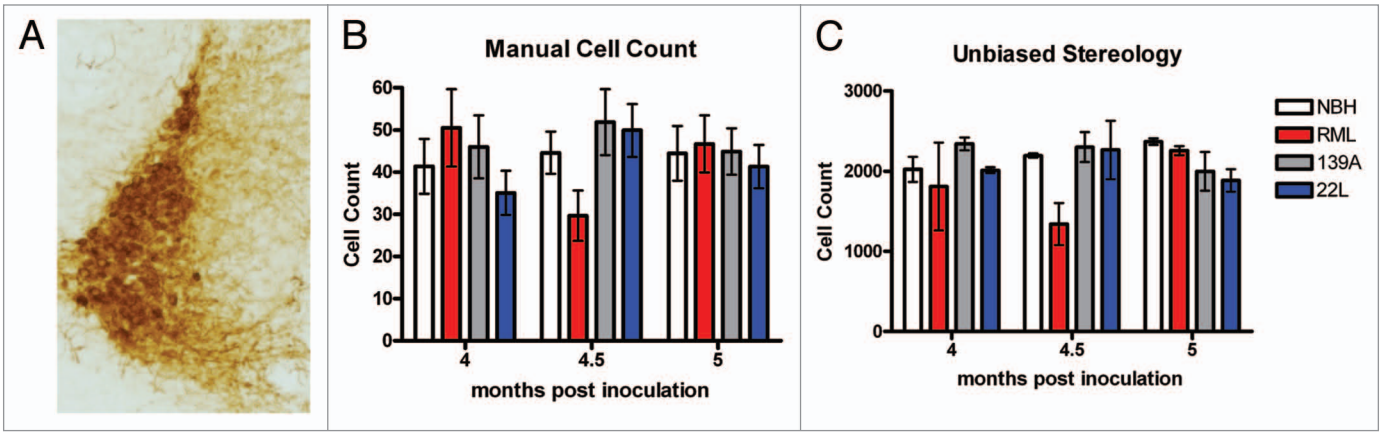

Figure 9. Quantification of TH-positive noradrenergic neurons in the locus coeruleus. (A) Representative image of TH staining in the locus coeruleus. (B) Manual cell counts and (C) unbiased stereology in the locus coeruleus (Kruskal-Wallis test with post-test) (*$p < 0.05$; **$p < 0.01$; ***$p < 0.001$).

"Chandler" strain of scrapie.[31] Dell'Omo et al.[32] conducted a similar comparative prion strain study, using laser-beam breaks to determine activity levels caused by of several different prion stains inoculated into C57BL/6 female mice. In their study 139A caused a hyperactivity phenotype in the home cage but of considerably smaller amplitude than what we observed whereas the other two strains that they tested, 301C and ME7, both caused rather dramatic hypoactivity (3-fold reduction in activity counts).[32] Thus, for some prion strains hypo- or hyperactivity will be an effective diagnostic with which to measure delays or accelerations in the disease progression.[6,10-12] One very clear change that we observed across all prion strains was a severe lack of hanging behavior, which either results from a lack of motivation or coordination required to hang from the wire food bin. This could serve as a useful general metric of prion disease either by hand scoring videos for those that do not have access to commercial home cage behavior monitoring systems such as HomeCageScan or through the use of a newly introduced open source software for home cage behavior recognition in mice.[33] It is also important to note that hamsters inoculated with either "hyper" or "drowsy" strains of transmissible mink encephalopathy as another clear case where prion strains differentially effect activity levels.[34-36]

The pathological markers, including glial stains and degeneration staining, revealed striking alterations in all prion-inoculated mice at or before the time at which symptoms appear whereas there was relatively little or no evidence for loss of neuromodulatory systems, including dopaminergic, serotonergic or noradrenergic neurons and the projections that we examined. Astro- and microglia showed a very strong concordance in most of the areas, showing essentially super imposable relative changes except for the higher baseline level of IBA1 positive microglia in NBH controls. Why might astrocytosis or microgliosis be more sensitive of a marker of disease than loss of cells types? Interestingly, dysfunction can be dissociated from death of cells by seizure induction, which in extreme forms lead to astrogliosis without cell loss.[16] Interestingly, Cunningham and colleagues also conducted a comparative study of several different prion strains, ME7, 79A and 22L.[37] Their major conclusion was that the behavioral and pathological onset of these diverse prion strains was quite similar in C57BL/6 female mice, whereas in our study, the pathology and behavior of 22L-inoculated mice was clearly different from RML and 139A.

Given the hyperactivity phenotype of RML- and 139A-inoculated mice; we focused our neuropathological investigation on brain regions controlling locomotor behavior. We were not able to pinpoint the population(s) of neurons responsible for the major behavioral phenotype of RML and 139A but did discern clear-cut changes in glial and degeneration staining and a slightly decreased dopamine innervation of the dorsal striatum. It is important to note that the glial markers for neuropathology were increased in 22L brains at 5 mpi, showing that gliosis in the dorsal striatum is not sufficient to induce hyperactivity. It is our interpretation that early gliosis is a specific marker of pathology but that later in disease gliosis is increased in so many regions that it is not very useful for identification of pathological lesions. Numerous alterations to the striatal neurons, which are typically GABAergic inhibitory neurons expressing either a D1 or a D2 dopamine receptor,[19] lead to hyperactivity.[26,38-41] Given that

dopamine promotes locomotor behavior, it has been a surprising but well documented result that decreases in the nigro-striatal dopamine system can actually increase locomotor behavior. In Pitx3 knockout mice there is a significant loss of DA neurons; yet, there is a hyperactivity phenotype that likely is caused by a compensatory increase in serotonergic innervations of the striatum,[42] which did not occur in our system (**Fig. 6**). Moreover, cholinergic neurons within the dorsal striatum or that project to locomotor regions also appear intact in RML- and 139A-inoculated animals, despite precedence for the importance of cholinergic neurons in determining locomotor activity levels.[27,28,43] In future studies it will be crucial to examine synaptic pathology, as done elegantly in models of prion disease by O'Connor and Perry in a series of studies[44-47] as it is possible that although neurotransmitter phenotypes are intact in terms of cell numbers, synapses may no longer be intact or functional. However, a method more rapid, such as immunostaining, than electron microscopy would be desirable for laboratories not equipped for such studies.

Given the recent connections[48-51] or lack thereof[52-55] found between prion and other neurodegenerative diseases, such as Alzheimer disease; it will be of great interest and importance to tease apart the molecular mechanism of prion pathology.[56] With a more standardized approach such as that taken here or in other studies,[32,37] comparing results between laboratories and replicating published results will be facilitated greatly.

Materials and Methods

Home cage behavior measurement and data analysis. 3-month old C57BL/6J females were purchased from the Jackson Laboratory. The mice were inoculated intracranially with a 26 gauge needle with either 5.5 log LD_{50} RML "Chandler", 0.1% weight per volume 139A (exact titer not determined) and 5.7 log LD_{50} 22L or 0.1% normal brain homogenate in phosphate buffered saline as a control (30 ul total injection volume). The mice were group housed except for when they were video recorded at 1, 3, 3.5, 4, 4.5, 5 and 5.5 mpi and on a 12:12 light:dark cycle. The same mice were used for survival and behavioral analysis and the sample sizes were between 12 and 13 mice for all groups. Female mice were chosen since this minimized the risk of fighting in this single to group housing situation. The videos were analyzed using HomeCageScan 2.0, a software for automated detection of home cage behaviors, using settings and behavioral definitions essentially as described in Steele et al. 2007.[57]

Figure 3 was generated using MATLAB R2008a using the travel data and the seconds per bin output from HomeCageScan analysis of 24 h video recordings. **Figure 3A** was generated using the MATLAB function AREA on a three-dimensional array containing the median value of each behavior for all mice in each experimental group at each hour bin and each month. **Figure 3B** was generated using the MATLAB function CONTOURF on array containing the median value of distance travelled for all mice in each experimental group at each hour bin and each month.

Graphs for behavioral data and histological data were prepared using GraphPad Prism and statistical tests were run using GraphPad InStat.

Histological analysis. For histology, mice were overdosed with avertin anesthetic and perfused transcardially with phosphat-buffered saline. Two mice from each group were sacrificed at 4, 4.5, 5 and 5.5 mpi. The brains were immersion fixed in 10% buffered formalin (Sigma). Upon receipt of the brain tissue at NeuroScience Associates, they were treated with 20% glycerol and 2% dimethylsulfoxide to prevent freeze-artifacts. They were then multiply embedded with up to 25 brains per block in a gelatin matrix using MultiBrain Technology™. The block of embedded tissue was allowed to cure and then was rapidly frozen by immersion in isopentane chilled to -70°C with crushed dry ice. Blocks were mounted on a freezing stage of an AO 860 sliding microtome and sectioned coronally at 35 μ thickness. All sections cut were collected sequentially into a 4 x 6 array of containers filled with "antigen preserve" (buffered ethylene glycol). At the completion of sectioning, each container holds a serial set of one-of-every-24th section (e.g., one section every 840 μ).

For immunochemistry, the sections were stained free-floating. All incubation solutions from the blocking serum onward use Tris-buffered saline (TBS) with Triton X100 (TX) as the vehicle; all rinses are with TBS. After a hydrogen peroxide treatment and blocking serum, the sections were immunostained with a primary antibody overnight at room temperature. Vehicle solution contains 0.3% TritonX-100 for permeabilization. Following rinses a secondary antibody (anti IgG of host animal in which the primary antibody was produced) that is biotinylated is applied. To visualize the location of binding site of the primary antibody an avidin-biotin-HRP complex (details in Vectastain elite ABC kit, Vector, Burlingame, CA) is applied. After rinses, the sections were treated with diaminobenzidine tetrahydrochloride (DAB) and hydrogen peroxide to create a visible reaction product and mounted on gelatinized (subbed) glass slides, air-dried, dehydrated in alcohols, cleared in xylene and coverslipped.

The following antibodies were used: rabbit anti-GFAP (DAKO) 1:20,000; rabbit anti-IBA1 (WAKO) 1:15,000; mouse anti-calbindin (Swant) 1:500; goat anti-ChAT (Chimicon, AB144P) 1:1,000; Rabbit anti-5-HT (Immunostar) 1:750,000; Rabbit anti-TH (Pelfreez) 1:6,000 and rabbit anti-parvalbumin (Swant) 1:500 for immunofluorescent staining with secondary antibody purchased from InVitrogen.

The Amino cupric silver staining closely followed the protocol described by deOlmos.[58] In brief, the free-floating sections were taken through the following major steps: pre-impregnation, impregnation, reduction, bleaching and fixing. The pre-impregnation solution contains cupric nitrate, silver nitrate, cadmium nitrate, lanthanum nitrate, Neutral Red, alpha-amino butyric acid, alanine, pyridine, triethanolamine, isopropanol and deionized water (dH_2O). After the components were well mixed, the solution was microwaved until it reached 45–50°C. The solution was left to cool to room temperature, then filtered. The sections

were removed from the antigen preserve solution and rinsed with dH_2O. The sections were then placed into dishes containing the pre-impregnation solution and heated in the microwave to 45–50°C. To allow for cooling, the sections remained in this solution overnight. The impregnation solution contains silver nitrate, 100% Ethanol, acetone, lithium hydroxide, ammonium hydroxide and dH_2O. The sections were rinsed first in dH_2O, secondly in acetone, and then placed into the Impregnation solution. The sections incubate in this solution for 50 min. The reducer solution contains 100% ethanol, formalin, citric acid and dH_2O. The sections were transferred from the impregnation solution into the reducer solution and placed in a water bath with a maintained temperature between 32–35°C. After 25 min in the reducer solution, the sections were transferred into dH_2O rinses. The bleaching solutions are potassium ferricyanide in potassium chlorate with lactic acid, potassium permanganate with sulfuric acid and sodium thiosulfate. The sections were rapidly transferred through these bleaching solutions, then fixed in Rapid Fixer Solution for 1 min 30 seconds. The sections were then rinsed in dH_2O, mounted on subbed glass slides and counterstained with Neutral Red to reveal normal cell bodies.

Cell counting. Cell counts in specific regions were performed using a Nikon Eclipse inverted microscope by first using 4x magnification to identify the appropriate field and anatomy for degeneration and gliosis (dorsal striatum), TH (SNc, dorsal striatum and LC), 5HT (DRN, dorsal striatum and SNc/r), ChAT (dorsal striatum, PPTg, LDTg). For densitometry, 10x magnification was used for degeneration and gliosis (dorsal striatum), TH (dorsal striatum), 5HT (dorsal striatum and SNc/r), ChAT (dorsal striatum). Manual cell counts for TH (SNc and LC), 5HT (DRN), ChAT (dorsal striatum, PPTg, LDTg) and Parvalbumin (dorsal striatum and SNc/r) were performed using 20x magnification. 10x magnification was used to count cells for TH (LC). Cells were counted manually using a clicker to record cell counts. Representative anatomies were captured by identifying the most rostral and caudal slides containing the relevant anatomy and counting any slides in between. The data presented in the graphs represents the mean and standard error of the mean calculated from anatomical counts of two biological replicates.

For computer assisted analysis of staining, Nikon Elements (www.nis-elements.com/) software was used. User input determined thresholds for counting positive staining and were and examples of staining thresholds are shown in **Figures 4C, 4F, 4M, 5F, 6F, 6J** and **8F**.

For the stereological analyses, the reference spaces on each sampled section were outlined under low-power magnification (4x) and total number of Iba-1-immunopositive microglia and TH-immunopositive neurons were quantified using a high resolution, oil immersion objective (60x, 1.4 numerical aperture). Neurons in the LC were identified on the basis of neuronal phenotype, i.e., a nucleolus and a well-formed nuclear membrane and TH immunoreactivity. Microglia in the dorsal striatum were identified on the basis of glial phenotype and Iba1 immunoreactivity. To avoid artifacts at the sectioning surface, e.g., lost caps, a guard volume was observed up to 1.5 um above and below the dissector where no cells were counted. Sampling of all parameters was continued to a mean coefficient of error (CE) of 0.05 to 0.10, according to Gundersen et al.[59] All stereological parameters were quantified with assistance from a computerized stereology system (Stereo Investigator, MBF Bioscience, Williston, VT) by an operator blind to treatment and according to established principles, as detailed previously.[60]

Acknowledgment

We thank Susan Lindquist for providing the 22L and RML prion strains, Claudio Hetz for providing 139A prions and Henry Lester for helpful advice. This work was funded by the Broad Fellows in Brain Circuitry Program at Caltech.

References

1. Aguzzi A, O'Connor T. Protein aggregation diseases: pathogenicity and therapeutic perspectives. Nat Rev Drug Discov 2010; 9:237-48.
2. Aguzzi A, Calella AM. Prions: protein aggregation and infectious diseases. Physiol Rev 2009; 89:1105-52.
3. Prusiner SB. Prions. Proc Natl Acad Sci USA 1998; 95:13363-83.
4. Prusiner SB. Novel proteinaceous infectious particles cause scrapie. Science 1982; 216:136-44.
5. Wang F, Wang X, Yuan CG, Ma J. Generating a prion with bacterially expressed recombinant prion protein. Science 2010; 327:1132-5.
6. Jackson WS, Borkowski AW, Faas H, Steele AD, King OD, Watson N, et al. Spontaneous generation of prion infectivity in fatal familial insomnia knockin mice. Neuron 2009; 63:438-50.
7. Sigurdson CJ, Nilsson KP, Hornemann S, Heikenwalder M, Manco G, Schwarz P, et al. De novo generation of a transmissible spongiform encephalopathy by mouse transgenesis. Proc Natl Acad Sci USA 2009; 106: 304-9.
8. Aguzzi A, Heikenwalder M, Polymenidou M. Insights into prion strains and neurotoxicity. Nat Rev Mol Cell Biol 2007; 8:552-61.
9. Morales R, Abid K, Soto C. The prion strain phenomenon: molecular basis and unprecedented features. Biochim Biophys Acta 2007; 1772:681-91.
10. Steele AD, Hetz C, Yi CH, Jackson WS, Borkowski AW, Yuan J, et al. Prion pathogenesis is independent of caspase-12. Prion 2007; 1:243-7.
11. Steele AD, King OD, Jackson WS, Hetz CA, Borkowski AW, Thielen P, et al. Diminishing apoptosis by deletion of Bax or overexpression of Bcl-2 does not protect against infectious prion toxicity in vivo. J Neurosci 2007; 27:13022-7.
12. Steele AD, Hutter G, Jackson WS, Heppner FL, Borkowski AW, King OD, et al. Heat shock factor 1 regulates lifespan as distinct from disease onset in prion disease. Proc Natl Acad Sci USA 2008; 105:13626-31.
13. Chen D, Steele AD, Hutter G, Bruno J, Govindarajan A, Easlon E, et al. The role of calorie restriction and SIRT1 in prion-mediated neurodegeneration. Exp Gerontol 2008; 43:1086-93.
14. Riemer C, Schultz J, Burwinkel M, Schwarz A, Mok SW, Gultner S, et al. Accelerated prion replication in, but prolonged survival times of, prion-infected $CXCR3^{-/-}$ mice. J Virol 2008; 82:12464-71.
15. White MD, Farmer M, Mirabile I, Brandner S, Collinge J, Mallucci GR. Single treatment with RNAi against prion protein rescues early neuronal dysfunction and prolongs survival in mice with prion disease. Proc Natl Acad Sci USA 2008; 105:10238-43.
16. Khurgel M, Switzer RC, 3rd, Teskey GC, Spiller AE, Racine RJ, Ivy GO. Activation of astrocytes during epileptogenesis in the absence of neuronal degeneration. Neurobiol Dis 1995; 2:23-35.
17. Brendza RP, O'Brien C, Simmons K, McKeel DW, Bales KR, Paul SM, et al. PDAPP; YFP double transgenic mice: a tool to study amyloid-beta associated changes in axonal, dendritic and synaptic structures. J Comp Neurol 2003; 456:375-83.
18. Switzer RC, 3rd. Application of silver degeneration stains for neurotoxicity testing. Toxicol Pathol 2000; 28:70-83.
19. Kreitzer AC, Malenka RC. Striatal plasticity and basal ganglia circuit function. Neuron 2008; 60:543-54.
20. Graybiel AM. Habits, rituals and the evaluative brain. Annu Rev Neurosci 2008; 31:359-87.
21. Martin S, van den Buuse M. Phencyclidine-induced locomotor hyperactivity is enhanced in mice after stereotaxic brain serotonin depletion. Behav Brain Res 2008; 191:289-93.
22. Zhou FM, Liang Y, Salas R, Zhang L, De Biasi M, Dani JA. Corelease of dopamine and serotonin from striatal dopamine terminals. Neuron 2005; 46:65-74.
23. Vidal C, Herzog C, Haeberle AM, Bombarde C, Miquel MC, Carimalo J, et al. Early dysfunction of central 5-HT system in a murine model of bovine spongiform encephalopathy. Neuroscience 2009; 160:731-43.
24. Guentchev M, Hainfellner JA, Trabattoni GR, Budka H. Distribution of parvalbumin-immunoreactive neurons in brain correlates with hippocampal and temporal cortical pathology in Creutzfeldt-Jakob disease. J Neuropathol Exp Neurol 1997; 56:1119-24.

25. Belichenko PV, Miklossy J, Belser B, Budka H, Celio MR. Early destruction of the extracellular matrix around parvalbumin-immunoreactive interneurons in Creutzfeldt-Jakob disease. Neurobiol Dis 1999; 6: 269-79.
26. Avale ME, Faure P, Pons S, Robledo P, Deltheil T, David DJ, et al. Interplay of beta2* nicotinic receptors and dopamine pathways in the control of spontaneous locomotion. Proc Natl Acad Sci USA 2008; 105:15991-6.
27. Drenan RM, Grady SR, Steele AD, McKinney S, Patzlaff NE, McIntosh JM, et al. Cholinergic modulation of locomotion and striatal dopamine release is mediated by alpha6alpha4* nicotinic acetylcholine receptors. J Neurosci 2010; 30:9877-89.
28. Drenan RM, Grady SR, Whiteaker P, McClure-Begley T, McKinney S, Miwa JM, et al. In vivo activation of midbrain dopamine neurons via sensitized, high-affinity alpha6 nicotinic acetylcholine receptors. Neuron 2008; 60:123-36.
29. Sara SJ. The locus coeruleus and noradrenergic modulation of cognition. Nat Rev Neurosci 2009; 10: 211-23.
30. O'Neil JN, Mouton PR, Tizabi Y, Ottinger MA, Lei DL, Ingram DK, et al. Catecholaminergic neuronal loss in locus coeruleus of aged female dtg APP/PS1 mice. J Chem Neuroanat 2007; 34:102-7.
31. Bruce ME, Fraser H. Scrapie strain variation and its implications. Current Topics in Microbiology and Immunology 1991; 172:125-38.
32. Dell'Omo G, Vannoni E, Vyssotski AL, Di Bari MA, Nonno R, Agrimi U, et al. Early behavioural changes in mice infected with BSE and scrapie: automated home cage monitoring reveals prion strain differences. Eur J Neurosci 2002; 16:735-42.
33. Jhuang H, Garrote E, Yu X, Khilnani V, Poggio T, Steele AD, et al. Automated home-cage behavioral phenotyping of mice. Nature Communications 2010; 1:68.
34. Ayers JI, Kincaid AE, Bartz JC. Prion strain targeting independent of strain-specific neuronal tropism. J Virol 2009; 83:81-7.
35. Bessen RA, Marsh RF. Biochemical and physical properties of the prion protein from two strains of the transmissible mink encephalopathy agent. J Virol 1992; 66:2096-101.
36. Bessen RA, Marsh RF. Identification of two biologically distinct strains of transmissible mink encephalopathy in hamsters. J Gen Virol 1992; 73:329-34.
37. Cunningham C, Deacon RM, Chan K, Boche D, Rawlins JN, Perry VH. Neuropathologically distinct prion strains give rise to similar temporal profiles of behavioral deficits. Neurobiol Dis 2005; 18:258-69.
38. Sano H, Yasoshima Y, Matsushita N, Kaneko T, Kohno K, Pastan I, et al. Conditional ablation of striatal neuronal types containing dopamine D2 receptor disturbs coordination of basal ganglia function. J Neurosci 2003; 23:9078-88.
39. Gantois I, Fang K, Jiang L, Babovic D, Lawrence AJ, Ferreri V, et al. Ablation of D1 dopamine receptor-expressing cells generates mice with seizures, dystonia, hyperactivity and impaired oral behavior. Proc Natl Acad Sci USA 2007; 104:4182-7.
40. Unger EL, Eve DJ, Perez XA, Reichenbach DK, Xu Y, Lee MK, et al. Locomotor hyperactivity and alterations in dopamine neurotransmission are associated with overexpression of A53T mutant human alpha-synuclein in mice. Neurobiol Dis 2006; 21:431-43.
41. Kelly MA, Rubinstein M, Phillips TJ, Lessov CN, Burkhart-Kasch S, Zhang G, et al. Locomotor activity in D2 dopamine receptor-deficient mice is determined by gene dosage, genetic background and developmental adaptations. J Neurosci 1998; 18:3470-9.
42. Smits SM, Noorlander CW, Kas MJ, Ramakers GM, Smidt MP. Alterations in serotonin signalling are involved in the hyperactivity of Pitx3-deficient mice. Eur J Neurosci 2008; 27:388-95.
43. Gomeza J, Zhang L, Kostenis E, Felder C, Bymaster F, Brodkin J, et al. Enhancement of D1 dopamine receptor-mediated locomotor stimulation in M(4) muscarinic acetylcholine receptor knockout mice. Proc Natl Acad Sci USA 1999; 96:10483-8.
44. Gray BC, Siskova Z, Perry VH, O'Connor V. Selective presynaptic degeneration in the synaptopathy associated with ME7-induced hippocampal pathology. Neurobiol Dis 2009; 35:63-74.
45. Siskova Z, Mahad DJ, Pudney C, Campbell G, Cadogan M, Asuni A, et al. Morphological and functional abnormalities in mitochondria associated with synaptic degeneration in prion disease. Am J Pathol 2010; 177:1411-21.
46. Siskova Z, Page A, O'Connor V, Perry VH. Degenerating synaptic boutons in prion disease: microglia activation without synaptic stripping. Am J Pathol 2009; 175:1610-21.
47. Siskova Z, Sanyal NK, Orban A, O'Connor V, Perry VH. Reactive hypertrophy of synaptic varicosities within the hippocampus of prion-infected mice. Biochem Soc Trans 2010; 38:471-5.
48. Lauren J, Gimbel DA, Nygaard HB, Gilbert JW, Strittmatter SM. Cellular prion protein mediates impairment of synaptic plasticity by amyloid-beta oligomers. Nature 2009; 457:1128-32.
49. Gimbel DA, Nygaard HB, Coffey EE, Gunther EC, Lauren J, Gimbel ZA, et al. Memory impairment in transgenic Alzheimer mice requires cellular prion protein. J Neurosci 2010; 30:6367-74.
50. Chen S, Yadav SP, Surewicz WK. Interaction between human prion protein and amyloid-beta (Abeta) oligomers: role OF N-terminal residues. J Biol Chem 2010; 285:26377-83.
51. Kellett KA, Hooper NM. Prion protein and Alzheimer disease. Prion 2009; 3:190-4.
52. Balducci C, Beeg M, Stravalaci M, Bastone A, Sclip A, Biasini E, et al. Synthetic amyloid-beta oligomers impair long-term memory independently of cellular prion protein. Proc Natl Acad Sci USA 2010; 107:2295-300.
53. Steele AD, Zhou Z, Jackson WS, Zhu C, Auluck P, Moskowitz MA, et al. Context dependent neuroprotective properties of prion protein (PrP). Prion 2009; 3:240-9.
54. Calella AM, Farinelli M, Nuvolone M, Mirante O, Moos R, Falsig J, et al. Prion protein and Abeta-related synaptic toxicity impairment. EMBO Mol Med 2010; 2:306-14.
55. Jeong BH, Lee KH, Jeong YE, Hwang KA, Lee YJ, Carp RI, et al. Polymorphisms at codons 129 and 219 of the prion protein gene (PRNP) are not associated with sporadic Alzheimer's disease in the Korean population. Eur J Neurol 2007; 14:621-6.
56. Cushman M, Johnson BS, King OD, Gitler AD, Shorter J. Prion-like disorders: blurring the divide between transmissibility and infectivity. J Cell Sci 2010; 123:1191-201.
57. Steele AD, Jackson WS, King OD, Lindquist S. The power of automated high-resolution behavior analysis revealed by its application to mouse models of Huntington's and prion diseases. Proc Natl Acad Sci USA 2007; 104:1983-8.
58. de Olmos JS, Beltramino CA, de Olmos de Lorenzo S. Use of an amino-cupric-silver technique for the detection of early and semiacute neuronal degeneration caused by neurotoxicants, hypoxia and physical trauma. Neurotoxicol Teratol 1994; 16:545-61.
59. Gundersen HJ, Jensen EB, Kieu K, Nielsen J. The efficiency of systematic sampling in stereology—reconsidered. J Microsc 1999; 193:199-211.
60. Manaye KF, Wang PC, O'Neil JN, Huang SY, Xu T, Lei DL, et al. Neuropathological quantification of dtg APP/PS1: neuroimaging, stereology and biochemistry. Age (Dordr) 2007; 29:87-96.